

Date of publication xxxx 00, 0000, date of current version xxxx 00, 0000.

Digital Object Identifier 10.1109/ACCESS.2017.DOI

3D Determination of Message Collection and Delivery Locations for UAV-Enabled Disaster Recovery Networks

AZUSA DANJO¹, SHINSUKE HARA¹, (Member, IEEE), TAKAHIRO MATSUDA², (Member, IEEE), FUMIE ONO³, (Member, IEEE), and RYU MIURA⁴, (Member, IEEE)

¹Graduate School of Engineering, Osaka City University, Osaka, Japan (e-mail: {danjo@c., hara@}info.eng.osaka-cu.ac.jp)

²Graduate School of Systems Design, Tokyo Metropolitan University, Tokyo, Japan (e-mail: takahiro.m@tmu.ac.jp)

³Ministry of Internal Affairs and Communications, Tokyo, Japan

⁴Wireless Networks Research Center, National Institute of Information and Communications Technology, Kanagawa, Japan

Corresponding author: Azusa Danjo (e-mail: danjo@c.info.eng.osaka-cu.ac.jp).

This study was supported in part by a Grant-in-Aid for Scientific Research (JP18H01445, JP19H04096) from the Ministry of Education, Science, Sport, and Culture of Japan, the ICOM Foundation, Japan, the Japanese Ministry of Internal Affairs and Communications in R & D on Cooperative Technologies and Frequency Sharing Between Unmanned Aircraft System (UAS)-Based Wireless Relay Systems and Terrestrial Networks, and TMU local 5G research support.

ABSTRACT When a large-scale disaster happens, critical infrastructure is destroyed, and many people are displaced. Unmanned aerial vehicle (UAV)-enabled disaster recovery networks can be used to support people in disaster-hit areas. However, determining UAV routes is critical to communicate with refugees. In this work, we propose a method to determine UAV locations to collect and deliver messages for UAV-enabled disaster recovery networks. Our method involves two stages: the received signal strength sensing stage and the message collection and delivery stage. We theoretically analyzed the computational complexity in terms of the number of steps and consequently evaluated the performance of our method using experimental data obtained from rural, suburban, and urban areas.

INDEX TERMS Correlation, Received signal strength, Tensor completion, and Unmanned aerial vehicles.

I. INTRODUCTION

NATURAL disasters such as earthquakes, floods, hurricanes, wildfires, and tornadoes have been increasing recently, partly because of global warming, which has increased the global temperature to its highest level in the past millennium [1].

Large-scale disasters displace many people, forcing them to live as refugees in shelters. For refugees, it is of utmost importance to communicate with their families about their situation as early as possible. However, terrestrial information networks often fail to function in these emergencies. For example, 400,000 people were displaced due to the 2011 Great Japan Earthquake, and terrestrial information networks perfectly became operational after more than a month [2]. Therefore, information network systems, which can be quickly constructed without infrastructure, are critical for disaster recovery.

Moreover, recent advancements in unmanned aerial vehicle (UAV) play an essential role in various commercial applications and wireless communication networks, such as

the fifth-generation (5G) network [3]. One of the advantages of UAVs is that they can fly anywhere with great flexibility, efficiency, and speed, which are highly needed for disaster recovery [4]. Let us consider UAV-enabled disaster recovery network involving one or more UAVs starting from a countermeasure office, visiting shelters to collect information from and deliver it to refugees, and returning to the office. In the case of ground logistics, ordering shelters in a time- and energy-efficient way has been well-discussed using the vehicle routing problem (VRP) [5], [6]. The main difference between ground logistics and aerial communication is that an automobile can visit a predetermined location in the two-dimensional (2D) plane to serve each person, whereas a UAV can freely visit an energy-efficient location in the three-dimensional (3D) region to collect and deliver messages for each shelter. Thus, determining UAV locations for message collection and delivery needs to be addressed to wirelessly collect and deliver messages for refugees.

UAVs have the 3D mobility but typically operate for up to 40 min [7] due to their limited battery capacity. To visit as

many shelters as possible in a short period, it is necessary to reduce energy consumption by shortening the time required for message collection and delivery and flying. If a UAV directly accesses individual refugees in a shelter, it would take longer, since a long connection time usually accompanies in each access. Therefore, pre-installing a server in each shelter to store all messages at once and send them in bulk using a UAV can save energy. In Japan, for an area that will presumably be damaged by a Nankai Trough earthquake, servers have been installed in some shelters and can communicate with UAVs as delay-tolerant network ferries [8].

Another energy-saving approach is to determine a UAV location where a better wireless link condition is obtained between the UAV and each server. In most wireless communication standards, the data transmission rate increases as the received signal strength (RSS) increases. Thus, the UAV should come closer to each server. However, this is not energy-efficient since the UAV consumes more energy for rising [9], and the flight time is prolonged due to the extended route length. Consequently, the UAV can be designed to collect and deliver messages for refugees while hovering over the shelter where the RSS is higher. Furthermore, in an area with multiple concentrated shelters, determining a UAV location to collect and deliver messages for multiple servers in bulk can be less time-consuming.

In a disaster-hit area, let us assign a 3D region with multiple servers to a UAV. Similar to a 2D or 3D geographical map used in ground logistics and transportation, the UAV uses a 3D RSS map to determine UAV locations for message collection and delivery. However, unlike a geographical map, the RSS map is server location-dependent, so spatial RSS sensing is required server by server. Because RSS sensing all over the region is extremely energy-consuming, the UAV should construct RSS maps for multiple servers by sparsely sensing RSSs while following a pre-determined route. In this case, we should note that the UAV can sense an RSS only for one server at a time, and even if the UAV stops at a targeted location for a while, it cannot always sense all RSSs [10] due to extremely low RSS values, packet collisions, and channel scanning mismatches.

In this work, we propose a method for determining UAV locations to collect and deliver messages for UAV-enabled disaster recovery networks. The proposed method involves two stages: the RSS sensing stage and the message collection and delivery stage. In the RSS sensing stage, 3D RSS maps are constructed for multiple servers from sparsely sensed RSS data through tensor completion. In the message collection and delivery stage, fewer locations adequate for multiple servers are determined by solving a combinatorial problem through utilizing normalized cross-correlations among constructed RSS maps to reduce computational complexity.

This article is organized as follows: Section II provides a literature review on UAV-enabled disaster recovery networks, VRP for UAVs, and RSS maps. Section III presents the models and assumptions, and Section IV provides the problem statement. Section V includes the tensor completion-based

method for constructing RSS maps. Section VI provides the correlation-based method for determining message collection and delivery locations. Section VII involves the evaluation of the proposed method using experimental data obtained in rural, suburban, and urban areas. Finally, Section VIII presents the conclusions of the work.

II. RELATED WORK

In recent years, several studies have been conducted on UAV-enabled disaster recovery networks. In [4], a cluster-based 2D framework for UAV locations was proposed. In [11], using node locations, 2D formation for UAVs was considered. Hourani *et al.* [12] proposed the optimal altitude to achieve maximum coverage area on the ground using a statistical propagation model that depends on the environment and the elevation angle from users. Moreover, UAV-based 3D location determination was investigated for wireless base stations in [13]– [15]. In [13], a circle packing-based method to maximize the total coverage area was proposed. Alzenad *et al.* [14] attempted to maximize the number of users within the coverage area using the minimum required transmitted power. In [15], by optimizing the UAV locations, the number of UAVs was minimized. Wang *et al.* [16] formulated a problem of altitude and power control using channel models of UAVs, satellites, and base stations. They discussed selecting a UAV as a gateway in flying ad hoc networks [17]. These problems are also discussed in the fifth-generation (5G) network and beyond [3], [18].

3D wireless channels may complicate channel conditions because of surrounding buildings. When the wireless channel condition is significantly affected by the distribution of surrounding buildings, it is difficult to correctly find UAV locations with better the conditions using statistical models. By using 3D RSS maps, we can find the optimal UAV locations because the estimated 3D RSS map includes the effect of surrounding buildings. Therefore, in this work, we focus on constructing 3D RSS maps using UAV.

Moreover, as aerial relay stations, UAVs play a critical role in wireless sensor networks (WSNs) [19]– [23]. In a WSN, UAVs wirelessly collect data from stationary sensors and deliver them to the base station. Therefore, the UAV routing problem is formulated as a VRP or a traveling salesman problem (TSP) [24], which is a special case of the VRP. In [21], the data acquisition latency was reduced using a modified nearest neighbor (NN) algorithm, where the NN algorithm is typically used to solve the TSP. In [22], [23], to extend the network lifetime, energy-efficient algorithms were proposed. Dorling *et al.* [25] considered a VRP in a UAV delivery problem and showed that the energy consumption of the UAV was proportional to the payload and battery weight. In [26], considering multiple charging stations and battery recharge on the way to collect and deliver packages, an algorithm to solve the VRP for multiple UAVs was proposed. In [27], with a UAV's power consumption model based on measured data, the minimization of energy consumption was formulated. In this problem, the UAV heading speed and

route were optimized by taking a shorter flying time and vulnerability to wind into consideration. In this work, we also considered the UAV routing problem and solved it with a TSP algorithm. However, our proposed method reduces the total route length by reducing the number of points for sensing through the tensor completion-based 3D RSS map estimation.

RSS maps can be used to design UAV locations or the UAV routing problem because they provide the spatial structure of shadowing due to surrounding obstacles in the 3D space. In [28], with an RSS map generated by ray-tracing simulations, the 3D locations of UAVs was defined. In [29], a maximum likelihood-based segmented regression method was proposed for 3D RSS map estimation. In [30], a total variation and low-rank tensor completion [31] were applied to efficiently construct a 3D RSS map by sensing RSSs in the partial region. This work is an extension of [32], where the location of a UAV to collect and deliver messages was determined using RSS maps estimated by a tensor completion-based RSS estimator in [30]. In addition to the contributions provided in [32], multiple locations can be determined using our method. In the case of the determination of a single location, all transmitted signals with sufficiently higher RSSs cannot always be received. To solve this problem, we formulated the optimization problem with multiple locations. Note that the conventional method in [32] is a special case of the proposed method. In section VII, we evaluated the performance of the proposed method against the number of locations. Another advantage of our method is that in addition to the field experiments in the urban area in [32], we evaluated the proposed method based on field experiments conducted in rural and suburban areas.

In this work, we do not compare our proposed method with other methods because of the following two reasons. First, the proposed method is a type of *joint sensing and communication systems*, that is, it is composed of two stages: the RSS sensing stage to estimate an RSS map and the message collection and delivery stage to select locations of the UAV to collect and deliver messages. To the best of our knowledge, this is the first demonstration of such a system utilized for disaster recovery systems. Second, although several algorithms for the VRP have been studied in the literature [21]–[23], [26], the objective of the work was not to outperform these algorithms but show the framework of the joint system. In other words, existing heuristic algorithms can be applied to the proposed method. Therefore, in this work, to validate the proposed method, we evaluated the performances of the RSS sensing stage and the message collection and delivery stage compared with those of the full sensing method and the brute search method, respectively, which will be explained in the following sections.

Notation: We use bold uppercase Roman letters for sets, e.g., \mathbf{A} , bold uppercase italic letters for matrices, e.g., \mathbf{B} , bold lowercase Roman letters for column vectors, e.g., \mathbf{c} , bold uppercase Greek letters for families of sets, e.g., Δ and

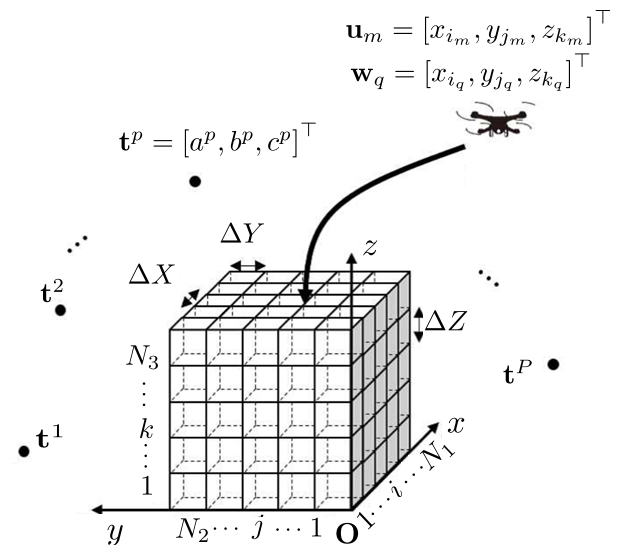


FIGURE 1. Layout model.

uppercase calligraphic letters for third-order tensors, e.g., \mathcal{E} , and we mean that lowercase italic subscripts are integers. In addition, we define \mathbf{f}^\top as the transposition of \mathbf{f} , $\mathbf{A} \oplus \mathbf{B}$ as the direct sum of \mathbf{A} and \mathbf{B} , and $|\mathbf{A}|$ as the cardinality of \mathbf{A} . Furthermore, we define $\|\mathbf{B}\|_*$ as the nuclear norm of \mathbf{B} , $\|\mathcal{G}\|_F$ as the Frobenius norm of \mathcal{G} , and $\|(\cdot)\|_n$ as the ℓ - n norm of (\cdot) , where (\cdot) can be a vector or matrix.

III. MODELS AND ASSUMPTIONS

A. SYSTEM MODEL

We assumed that multiple shelters were present in a disaster-hit area in which refugees have messages to transmit/receive and that a UAV with a wireless communication tool visits the area to collect and deliver messages while hovering over the area. In addition, we assumed that a server was installed in each shelter to temporarily store messages from refugees/UAV, so the UAV collects and delivers messages not directly from the refugees but via the server. Hereinafter, we refer to servers in shelters as *transceivers (TRXs)*.

Regarding the message collection and delivery process, we assumed that it was composed of two stages: the RSS sensing stage and the message collection and delivery stage. In the RSS sensing stage, the UAV senses RSSs for TRXs, and in the message collection and delivery stage, it collects and delivers messages at fewer locations selected according to the result of RSS sensing. Note that once adequate locations are determined, the RSS sensing stage can be skipped.

We considered that shelters were deployed in public areas such as elementary and junior high schools and parks. In Osaka City, Japan, more than 400 elementary and junior high schools are present within 223 km². We assumed that the schools were placed within a square area with a size of 223 km². In this case, the average distance between the two nearest schools was about 0.7 km. When the UAV flies at a speed of 40 km/h for 40 min [7], it can visit a maximum of

38 shelters with a full battery charge. We assumed that each stage was conducted by one UAV with a full battery charge. Multiple batteries or UAVs will be considered in future work.

B. LAYOUT MODEL

Fig. 1 shows the layout model involving a 3D region of interest, P stationary TRXs located out of it, and a UAV flying in it. The region has a size of $Xm \times Ym \times Zm$, and it is divided into $N_1 \times N_2 \times N_3 = N_v$ voxels with a size of $\Delta Xm \times \Delta Ym \times \Delta Zm$, where N_1 , N_2 , and N_3 denote the numbers of voxels dividing the region along directions of x , y , and z -axis, respectively. Defining the location of the center of gravity of the voxel as $\mathbf{g}_{ijk} = [x_i, y_j, z_k]^T$, we form the set of all \mathbf{g}_{ijk} 's as $\mathbf{G} = \{\mathbf{g}_{ijk} | 1 \leq i \leq N_1, 1 \leq j \leq N_2, 1 \leq k \leq N_3\}$, whose elements are simply referred to as *points*. In addition, defining the location of the p th TRX as $\mathbf{t}^p = [a^p, b^p, c^p]^T$, we form the set of all indexes for TRXs as $\mathbf{S} = \{p | 1 \leq p \leq P\}$.

In the RSS sensing stage, the UAV visits M points ($M \leq N_v$) out of \mathbf{G} along a predetermined route and senses RSSs for TRXs at each point. Defining the location of the m th RSS sensing point as $\mathbf{u}_m = [x_{i_m}, y_{j_m}, z_{k_m}]^T$, we form the set of all \mathbf{u}_m 's as $\mathbf{U} = \{\mathbf{u}_m | 1 \leq m \leq M\}$ ($\mathbf{U} \subseteq \mathbf{G}$). Here, RSS sensing efficiency is a key metric for the system, so we define the sensing rate as $E_{\text{sense}} = M/N_v$.

Note that the RSS in this work includes only a near-far effect determined by the locations of transceivers and shadowing determined by the surrounding environment, such as the distribution of buildings. In other words, the RSS does not include a time-varying fading effect. To construct an RSS map by 3D spatial sampling, its resolutions need to be short enough as compared with the decorrelation distance due to shadowing [33] as

$$\Delta X, \Delta Y, \Delta Z < d_{\text{decor}}. \quad (1)$$

Then, in the message collection and delivery stage, the UAV visits Q ($Q \leq M$) points out of \mathbf{U} along a predetermined route, and it collects and delivers messages at each point. Defining the location of the q th message collection and delivery point as $\mathbf{w}_q = [x_{i_q}, y_{j_q}, z_{k_q}]^T$, we form the set of all \mathbf{w}_q 's as $\mathbf{W} = \{\mathbf{w}_q | 1 \leq q \leq Q\}$ ($\mathbf{W} \subseteq \mathbf{U}$). In addition, defining the set of indexes for TRXs whose messages are collected and delivered at the q th point as \mathbf{S}_q with P_q elements, where P_q satisfies

$$\sum_{q=1}^Q P_q = P, \quad (2)$$

we form the family of all \mathbf{S}_q 's as $\mathbf{\Sigma} = \{\mathbf{S}_q | 1 \leq q \leq Q\}$. The UAV needs to collect and deliver a message for any TRX at a single point without duplication, so \mathbf{S} needs to be decomposed in the form of a direct sum as

$$\mathbf{S} = \bigoplus_{q=1}^Q \mathbf{S}_q. \quad (3)$$

TABLE 1. SYMBOLS AND NOTATIONS USED IN THIS WORK.

Notation	Definition
P	Number of TRXs
\mathbf{g}_{ijk}	Center of gravity of the voxel
N_v	Number of all voxels
\mathbf{G}	Set of all \mathbf{g}_{ijk} 's
\mathbf{t}^p	p th TRX
\mathbf{S}	Set of all indexes for TRXs
M	Number of UAV visit points
\mathbf{u}_m	m th RSS sensing point
\mathbf{U}	Set of all \mathbf{u}_m 's
E_{sense}	Sensing rate
\mathbf{w}_q	q th message collection/delivery point
Q	Number of \mathbf{w}_q
\mathbf{W}	Set of all \mathbf{w}_q 's
\mathbf{S}_q	Set of indexes for TRXs whose messages are collected/delivered at the q th point
P_q	Number of elements in \mathbf{S}_q
$\mathbf{\Sigma}$	Family of all \mathbf{S}_q 's
V_{uav}	UAV flying speed [m/sec]
L_{ab}	Link length from \mathbf{u}_a to \mathbf{u}_b [m]
$T_f(\mathbf{u}_a, \mathbf{u}_b)$	Time required for flying from \mathbf{u}_a to \mathbf{u}_b [sec]
C_{sense}	RSS sensing probability for the p th TRX at \mathbf{u}_m
\mathbf{B}^p	Set of sensing point indexes for the p th TRX
$R(\mathbf{u}_m, \mathbf{t}^p)$	RSS at \mathbf{u}_m for the p th TRX
\mathbf{R}^p	RSS map of the p th TRX
$T_s(\mathbf{u}_m)$	Time required for sensing RSSs at \mathbf{u}_m [sec]
$T_c(\mathbf{w}_q, \mathbf{t}^p)$	Message collection/delivery time [sec]
D_p	Total size of messages to collect/deliver [bit]

C. UAV MODEL

We assumed that the UAV was equipped with a global positioning system (GPS) receiver to exactly know its 3D location and a wireless communication tool to communicate with TRXs and that it flew at a constant speed (V_{uav}). In addition, we define the link length and period required for flying from \mathbf{u}_a to \mathbf{u}_b as $L_{ab} = \|\mathbf{u}_b - \mathbf{u}_a\|_2$ m and $T_f(\mathbf{u}_a, \mathbf{u}_b)$ s, respectively.

D. WIRELESS COMMUNICATION MODEL

In the RSS sensing stage, P TRXs transmit their wireless signals for the UAV, and the UAV tries to receive them to sense their RSSs. However, the UAV cannot receive all of them at each RSS sensing point, so we define the probability that the UAV can sense the RSS for the p th TRX at \mathbf{u}_m as C_{sense} .

By defining the set of indexes for the points where the UAV can sense RSSs for the p th TRX as \mathbf{B}^p , the RSS map of the p th TRX is given by

$$\mathbf{R}^p = \{R_{i_m j_m k_m}^p = R(\mathbf{u}_m, \mathbf{t}^p) | m \in \mathbf{B}^p\}, \quad (4)$$

where $R(\mathbf{u}_m, \mathbf{t}^p)$ denotes the RSS at \mathbf{u}_m for the p th TRX. We refer to the RSS map for $M = N_v$ and $C_{\text{sense}} = 1$ as the full RSS map and the one for $M < N_v$ as the partial RSS map. In addition, we defined the time required for sensing RSSs at \mathbf{u}_m as $T_s(\mathbf{u}_m)$ and assumed that $T_s(\mathbf{u}_m) \approx T_s$ ($1 \leq m \leq M$).

In the message collection and delivery stage, we defined the data transmission rate when collecting or delivering mes-

sages from the p th TRX at \mathbf{w}_q as $f(R(\mathbf{w}_q, \mathbf{t}^p))$. Defining the total size of messages to collect and deliver as D_p bit, although the messages may be fragmented, we assumed that the message collection and delivery time was given by

$$T_c(\mathbf{w}_q, \mathbf{t}^p) = D_p / f(R(\mathbf{w}_q, \mathbf{t}^p)). \quad (5)$$

When TRXs have data with different sizes, the data collection and delivery time may be longer than expected because the message collection and delivery stage does not provide the optimal solution in such a case. We considered two approaches to solve this problem. One was to formulate the optimization problem in the stage by taking account of the data size. The other was to fragment the messages of each TRX into data with a maximum size of D and collect and deliver messages over multiple rounds of the message collection and delivery stage. In this work, we considered the latter method, which is appropriate when all TRXs have sufficiently large data compared with D , and assumed that $D_p \approx D$ ($1 \leq p \leq P$).

IV. PROBLEM STATEMENT

A. RSS SENSING STAGE

When the UAV sequentially visits $\mathbf{u}_1, \mathbf{u}_2, \dots, \mathbf{u}_M$, the minimization of the total RSS sensing time is given by

$$\text{find } \hat{\mathbf{U}} \subseteq \mathbf{G} \text{ which minimizes} \\ T_{\text{total}} = \sum_{m=1}^M T_s(\mathbf{u}_m) + \sum_{m=1}^{M-1} T_f(\mathbf{u}_m, \mathbf{u}_{m+1}). \quad (6)$$

B. MESSAGE COLLECTION AND DELIVERY STAGE

When the UAV sequentially visits $\mathbf{w}_1, \mathbf{w}_2, \dots, \mathbf{w}_Q$, the minimization of the total message collection and delivery time is given by

$$\text{find } \hat{\mathbf{W}} \subseteq \mathbf{U}, \hat{\Sigma} \text{ which minimizes} \\ T_{\text{total}} = \sum_{q=1}^Q \sum_{p \in \mathbf{S}_q} T_c(\mathbf{w}_q, \mathbf{t}^p) + \sum_{q=1}^{Q-1} T_f(\mathbf{w}_q, \mathbf{w}_{q+1}). \quad (7)$$

V. SOLUTIONS IN RSS SENSING STAGE

In the RSS sensing stage, since $T_s(\mathbf{u}_m) \approx T_s$ and $T_f \gg T_s$, assuming constant UAV speed, we reformulated the minimization of the total route length as

$$\text{find } \hat{\mathbf{U}} \subseteq \mathbf{G} \text{ which minimizes} \\ L_{\text{total}} = \sum_{m=1}^{M-1} L_{m+1 m}. \quad (8)$$

A. PARTIAL SENSING (PS) AND FULL SENSING (FS) METHODS

We applied a solution method in the TSP to find the shortest RSS sensing route, where the UAV leaves \mathbf{u}_1 , visits M sensing points, and returns to $\mathbf{u}_{M+1} = \mathbf{u}_1$:

$$L_{\text{total}} = \sum_{m=1}^M L_{m+1 m}. \quad (9)$$

In detail, we randomly selected RSS sensing points $\mathbf{U}' = \{\mathbf{u}'_1, \mathbf{u}'_2, \dots, \mathbf{u}'_M\}$ out of \mathbf{G} and then reordered \mathbf{U}' so that L_{total} can be the shortest:

$$\text{randomly select } \mathbf{U}' \subseteq \mathbf{G} \\ \hat{\mathbf{U}} = \arg \min_{\mathbf{U}=\mathbf{U}'} L_{\text{total}}. \quad (10)$$

This method is referred to as the PS and FS methods, especially for $M = N_v$ and $C_{\text{sense}} = 1$. Note that the solution method is excluded from the scope of this work since many methods have been applied elsewhere for the TSP, such as the genetic algorithm [34] and the ant colony system [35].

B. TENSOR COMPLETION (TC) METHOD

Selected RSS sensing points do not give high RSSs for TRXs. As M decreases, the RSS sensing time becomes shorter; on the contrary, the message collection and delivery time becomes contrarily longer although Q increases. Thus, we proposed a method to shorten both the RSS sensing time and the message collection and delivery time based on tensor completion.

Defining a third-order tensor for the full RSS map of the p th TRX as

$$\mathcal{H}^p = \{H_{ijk} | 1 \leq i \leq N_1, \\ 1 \leq j \leq N_2, 1 \leq k \leq N_3\}, \quad (11)$$

the total-variation low-rank tensor completion method [31] constructs the full RSS map as ($1 \leq p \leq P$)

$$\hat{\mathcal{H}}^p = \arg \min_{\mathcal{H}^p} \lambda \sum_{n=1}^3 \|\mathbf{F}_n \mathbf{H}_{(n)}^p\|_1 \\ + (1 - \lambda) \frac{1}{3} \sum_{n=1}^3 \|\mathbf{H}_{(n)}^p\|_* \quad (12) \\ \text{subject to} \\ \mathbf{H}_{ijk}^p = \mathbf{R}_{i_m j_m k_m}^p \quad (m \in \mathbf{B}^p), \quad (13)$$

where $\mathbf{H}_{(n)}^p$ denotes the mode- n unfolding matrix of \mathcal{H}^p , and $\mathbf{F}_n = \{f_{l_1 l_2}\}$ denotes the smoothness constraint matrix, whose element is given by

$$f_{l_1 l_2} = \begin{cases} 1 & (l_2 = l_1) \\ -1 & (l_2 = l_1 + 1) \\ 0 & (\text{otherwise}) \end{cases} \quad (14)$$

with a changeable size according to $\mathbf{H}_{(n)}$, that is

$$\begin{aligned} 1 \leq l_1 \leq N_1, 1 \leq l_2 \leq N_2 \times N_3 & \quad (n = 1) \\ 1 \leq l_1 \leq N_2, 1 \leq l_2 \leq N_3 \times N_1 & \quad (n = 2) \\ 1 \leq l_1 \leq N_3, 1 \leq l_2 \leq N_1 \times N_2 & \quad (n = 3). \end{aligned} \quad (15)$$

The first and second terms of (12) indicate the total variation, and low-rank tensor completion, respectively and λ is a tunable parameter to balance them ($0 \leq \lambda \leq 1$). This method is referred to as the TC method, whose computational order is given by [36], [37]

$$O_{\text{TC}} = O(\max(N_1, N_2, N_3)^4). \quad (16)$$

VI. SOLUTION IN MESSAGE COLLECTION AND DELIVERY STAGE

In the message collection and delivery stage, since $T_c \gg T_f$, the minimization problem is simplified as

$$\text{find } \hat{\mathbf{W}} \subseteq \mathbf{U}, \hat{\Sigma} \text{ which minimizes}$$

$$T_{\text{total}} = \sum_{q=1}^Q \sum_{p \in \mathbf{S}_q} T_c(\mathbf{w}_q, \mathbf{t}^p). \quad (17)$$

In (17), the dominant factor to determine the message collection and delivery time at \mathbf{w}_q is the maximum of $T_c(\mathbf{w}_q, \mathbf{t}^p)$, namely, the minimum of $f(R(\mathbf{w}_q, \mathbf{t}^p))$. Therefore, by taking into consideration that $f(R(\mathbf{w}_q, \mathbf{t}^p))$ is an increasing function of $R(\mathbf{w}_q, \mathbf{t}^p)$, the problem is reformulated by the maximization of the sum of RSS as

$$\hat{\mathbf{W}}, \hat{\Sigma} = \arg \max_{\mathbf{W} \subseteq \mathbf{U}, \Sigma} R \quad (18)$$

$$R = \sum_{q=1}^Q R_q \quad (19)$$

$$R_q = \min_{p \in \mathbf{S}_q} R(\mathbf{w}_q, \mathbf{t}^p). \quad (20)$$

A. BRUTE SEARCH (BS) METHOD

One method is to pick up a combination of \mathbf{W} and Σ , which gives the maximal R in (18) out of all possible combinations. For the PS method without the TC method, to evaluate (20), it is necessary to check the condition whether the RSSs of the TRXs included in \mathbf{S}_q are sensible at \mathbf{w}_q , that is,

$$q \in \bigcap_{p \in \mathbf{S}_q} \mathbf{B}^p \quad (21)$$

for each of all the combinations of \mathbf{W} and Σ , which seems complicated. However, by adding RSS values low enough (typically -200 dBm) to be identified as *RSS-unsensible points* to the p th RSS map as

$$\tilde{\mathbf{R}}^p = \mathbf{R}^p \bigcup \{R_{i_m j_m k_m}^p = R_{\text{low}} | 1 \leq i_m \leq N_1, 1 \leq j_m \leq N_2, 1 \leq k_m \leq N_3, m \notin \mathbf{B}^p\} \quad (22)$$

R becomes searchable for all combinations of \mathbf{W} and Σ , and finally a solution automatically rejects RSS-unsensible points. This method is referred to as the BS method, whose computational order in terms of the number of steps is lower-bounded by (Appendix A)

$$O_{\text{BS}} = O(P \times M^Q). \quad (23)$$

Note that when M and Q are large, this method becomes unusable due to its extremely higher computational complexity.

B. CORRELATION (CO) METHOD

The normalized RSS correlation between \mathbf{R}^p and $\mathbf{R}^{p'}$ ($1 \leq p, p' \leq P, p \neq p'$) is defined as

$$\rho(\mathbf{R}^p, \mathbf{R}^{p'}) = \frac{\text{Cov}(\mathbf{R}^p, \mathbf{R}^{p'})}{\sigma_{\mathbf{R}^p} \sigma_{\mathbf{R}^{p'}}}, \quad (24)$$

where variables are averaged over only the RSS sensing points commonly included in \mathbf{B}^p and $\mathbf{B}^{p'}$ as

$$\frac{1}{|\mathbf{B}^p \cap \mathbf{B}^{p'}|} \sum_{m \in \mathbf{B}^p \cap \mathbf{B}^{p'}} (\cdot). \quad (25)$$

It is reasonable that the UAV can collect and deliver messages jointly for multiple TRXs with higher RSS correlations among them at a point; in other words, \mathbf{S} should be decomposed into subsets, where intra-subset elements have higher RSS correlations, whereas inter-subset elements have lower RSS correlations. Therefore, defining an RSS threshold as ρ_{th} , \mathbf{S} can be decomposed as

$$\text{find } \hat{\Sigma}$$

subject to

$$\begin{cases} \rho(\mathbf{R}^p, \mathbf{R}^{p'}) \geq \rho_{\text{th}} & (p, p' \in \mathbf{S}_q, p \neq p') \\ \rho(\mathbf{R}^p, \mathbf{R}^{p'}) < \rho_{\text{th}} & (p \in \mathbf{S}_q, p' \in \mathbf{S}_{q'}, p \neq p') \\ & (1 \leq q, q' \leq Q, q \neq q'). \end{cases}$$

This decomposition can be reformulated as a graph coloring problem (GCP) (Appendix B), and many solution methods have been proposed to solve the GCP [38].

When \mathbf{S}_q is given from (20), R_q is reduced to w_q . Therefore, by using $\hat{\Sigma} = \{\hat{\mathbf{S}}_q | 1 \leq q \leq Q\}$, we can divide the optimization problem (18), (19), and (20) into Q sub-problems, and \mathbf{w}_q ($q = 1, 2, \dots, Q$) is obtained by maximizing R_q instead of R :

$$\hat{\mathbf{w}}_q = \arg \max_{\mathbf{w}_q \in \mathbf{U}} R_q \quad (26)$$

$$R_q = \min_{p \in \hat{\mathbf{S}}_q} R(\mathbf{w}_q, \mathbf{t}^p). \quad (27)$$

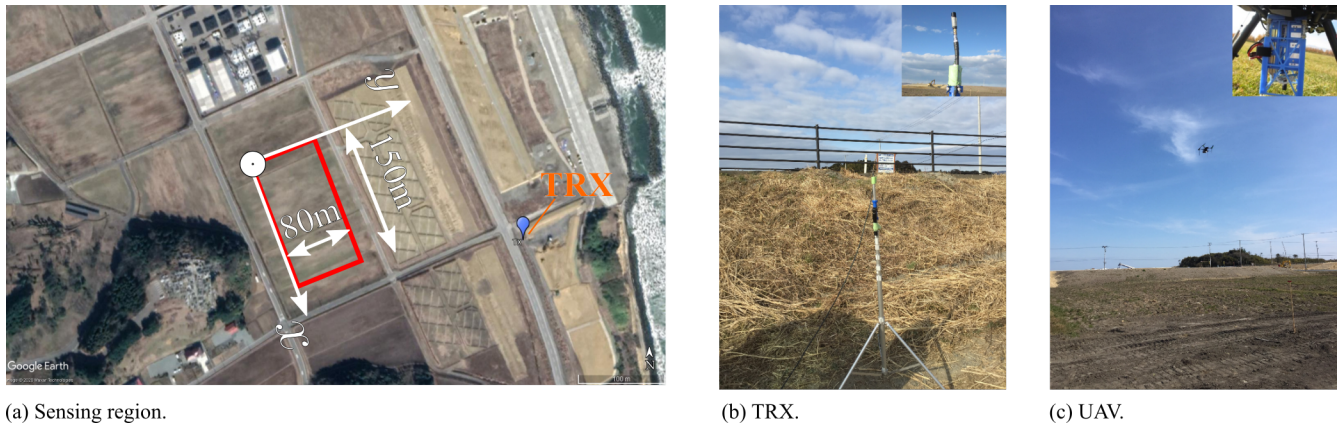
This method is referred to as the CO method, whose computational order is given by (Appendix C)

$$O_{\text{CO}} = O(P^2 \times M). \quad (28)$$

Note that the solution does not give the shortest route, so \mathbf{W} should be finally reordered to make the route the shortest.

TABLE 2. DETAIL ON THE FIRST EXPERIMENT CONDUCTED IN THE RURAL AREA.

Location	Mimamisouma City
Origin of the sensing region	Latitude: 37°31'12.99"N
	Longitude: 141°1'47.59"E
	Altitude: 10 m
Sizes of sensing region	$X = 150 \text{ m} \times Y = 80 \text{ m} \times Z = 40 \text{ m}$
Sensing resolution	$\Delta X = \Delta Y = \Delta Z = 10 \text{ m}$ $N_1 = 15, N_2 = 8, N_3 = 4,$ and $N_v = 480$
Number of TRXs (Q)	1
Wireless communication tool	5 GHz band PSK
Transmission power	30 dBm
Antenna	Vertically polarized dipole antenna
Antenna gain	2.14 dBi
UAV	Hexaroter

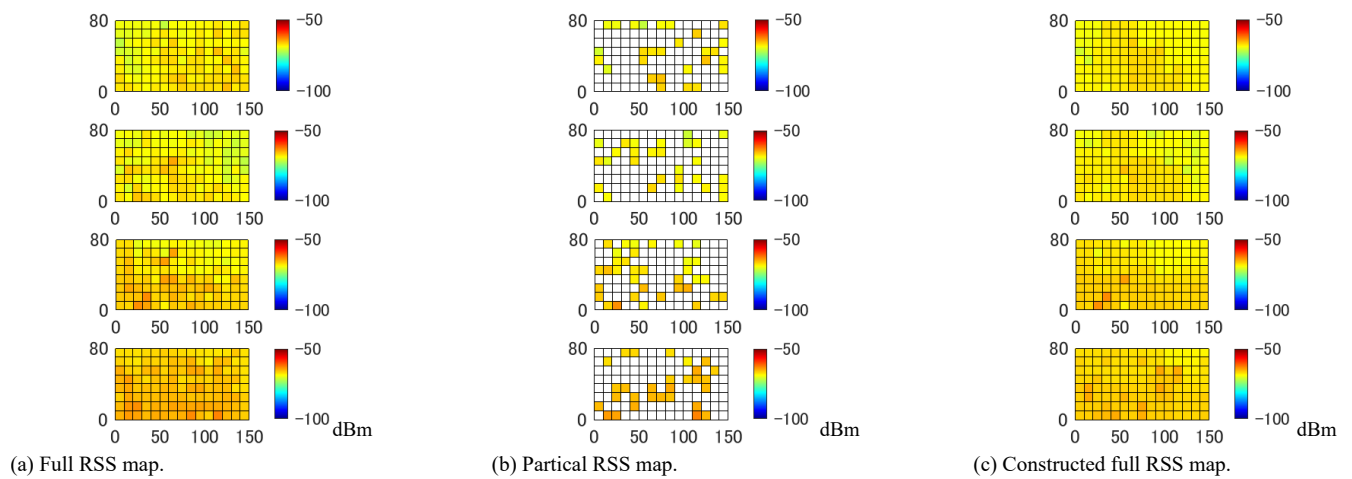


(a) Sensing region.

(b) TRX.

(c) UAV.

FIGURE 2. Photos of the first experiment, which was conducted in the rural area.



(a) Full RSS map.

(b) Partial RSS map.

(c) Constructed full RSS map.

FIGURE 3. RSS maps for $E_{\text{sense}} = 0.25$ and $\lambda = 0.07$ obtained from the first experiment, which was conducted in the rural area.

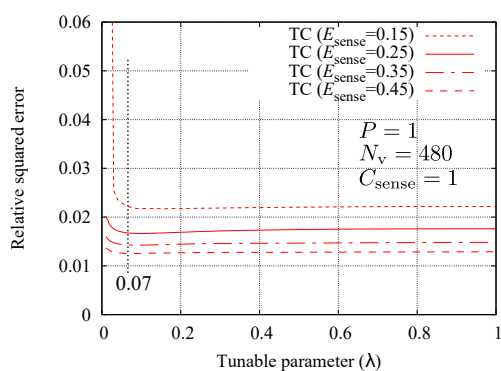


FIGURE 4. Dependency of the RSE on λ obtained from the first experiment, which was conducted in the rural area.

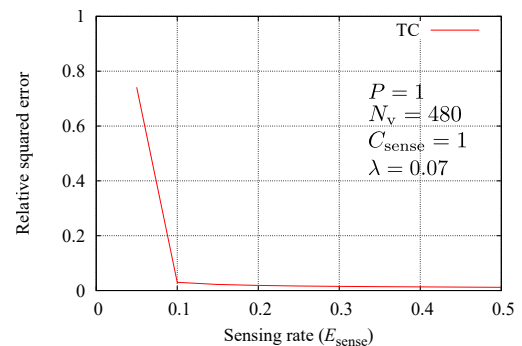


FIGURE 5. Dependency of the RSE on E_{sense} obtained from the first experiment, which was conducted in the rural area.

VII. PERFORMANCE EVALUATION

A. COMPARISON OF COMPUTATIONAL EFFICIENCIES

First, for the FS method combined with the BS method, by setting $M = N_v$ in (23), its computational order is lower-bounded by

$$O_{\text{FS/BS}} = O(P \times N_v^Q). \quad (29)$$

Second, for the PS method combined with the CO method, by setting $M = \lfloor E_{\text{sense}} \times N_v \rfloor$ in (28), its computational order is upper-bounded by

$$O_{\text{PS/CO}} = O(P^2 \times E_{\text{sense}} \times N_v). \quad (30)$$

Third, for the PS method combined with the CO and TC methods, since $\max(N_1, N_2, N_3)^4$ in (16) is usually much

larger than $P^2 \times E_{\text{sense}} \times N_v$ in (28), its computational order is given by

$$O_{\text{PS/TC/CO}} = O(\max(N_1, N_2, N_3)^4). \quad (31)$$

Comparing (29) with (30), if $E_{\text{sense}} < N_v^{Q-1}/P$, which is always satisfied when $Q > 1$, the PS/CO method is computationally more efficient than the FS/BS method.

Moreover, from (31), the computational order of the PS method combined with the CO and TC methods is region shape-dependent, but since

$$N_v^{\frac{1}{3}} \leq \max(N_1, N_2, N_3) \leq N_v \quad (32)$$

comparing (29) with (31), when $Q \gtrsim 3$, the PS/TC/CO method is computationally more efficient than the FS/BS method.

B. FIELD EXPERIMENTS

To evaluate the performance of the proposed method, we conducted experiments in rural, suburban, and urban areas. The first and second experiments were preliminary to confirm the relationship between the sensing rate of the PS method and the full RSS map constructability by the TC method, and the third experiment was to demonstrate the effectiveness of the CO method combined with the PS and TC methods. In each experiment, we predetermined the 3D spatial sampling resolutions to satisfy (1) (Appendix D).

As the performance metric of the full RSS map constructability, we used the relative square error (RSE) defined as

$$\text{RSE} = \frac{\sqrt{\sum_{p=1}^P \|\mathcal{H}^p - \tilde{\mathcal{H}}^p\|_F^2}}{\sqrt{\sum_{p=1}^P \|\mathcal{H}^p\|_F^2}}. \quad (33)$$

All performance metrics shown in the following figures are medians obtained over 1,000 random selections of RSS sensing points.

1) Rural Area

Figs. 2 (a)–(c) show the photos of the first experiment, where the sensing region was a rice field in a rural area. We placed a single TRX on the ground, and a UAV was used to sense its RSS. Table 2 summarizes the details of the experiment.

Figs. 3 (a)–(c) show the comparison of the full RSS map by the FS method, partial RSS map by the PS method, and full RSS map constructed from the partial RSS map by the TC method, where E_{sense} and λ are set to 0.25 and 0.07, respectively. The sensing region had a flat ground surface, but groves were located to the west and south of the land, so the effect of reflected wireless signals by them was observed in Fig. 3 (a). The RSS was simply not a monotonically decreasing function of the distance between the UAV and the TRX, in other words; some higher and lower RSS values were locally observed. Comparing the RSS maps in Figs. 3 (a) and (c), we deduced that by sensing RSSs in only 25% of the entire region, the TC method can construct the full RSS map well.

Figs. 4 and 5 show the dependencies of the RSE on λ and E_{sense} , respectively. We can see from these figures that the RSE improves as E_{sense} increases, where λ can minimize the RSE at around 0.1 for E_{sense} more than 0.25, and the RSE for E_{sense} more than 0.1 is sufficiently small.

TABLE 3. DETAIL ON THE SECOND EXPERIMENT CONDUCTED IN THE SUBURBAN AREA.

Location	Tarumizu city
Origin of the sensing region	Latitude: 31°30'55.11"N Longitude: 130°46'48.55"E Altitude: 30 m
Sizes of the sensing region	$X = 30 \text{ m} \times Y = 35 \text{ m} \times Z = 25 \text{ m}$
Sensing resolution	$\Delta X = \Delta Y = \Delta Z = 5 \text{ m}$ $N_1 = 6, N_2 = 7, N_3 = 5,$ and $N_v = 210$
Number of TRXs (Q)	1
Wireless communication tool	5 GHz band PSK
Transmission power	27 dBm
Antenna	Vertically polarized dipole antenna
Antenna gain	2 dBi
UAV	Hexaroter

2) Suburban Area

Figs. 6 (a)–(c) show the photos of the second experiment, where the sensing region was involved in a suburban area. We placed a single TRX on the ground and used a UAV to sense its RSS. Table 3 summarizes the details of the experiment.

Figs. 7 (a)–(c) show the comparison of the full RSS map, partial RSS map, and constructed full RSS map, where E_{sense} and λ are set to 0.25 and 0.07, respectively. Similar to the results in the first experiment, it seems that by sensing RSS in only 25% of the entire region, the TC method can construct the full RSS map well.

Figs. 8 and 9 show the dependencies of the RSE on λ and E_{sense} , respectively. In these figures, we can see tendencies similar to those in the first experiment, and especially, λ can minimize the RSE at around 0.1 for E_{sense} more than 0.25, as shown in Figs. 4 and 8, although the surrounding environments are different for the rural and suburban areas. We can also see from Fig. 9 that there is a threshold value for E_{sense} to minimize the RSE but the threshold of 0.15 in Fig. 9 is higher than that of 0.1 in Fig. 5 because the RSS fluctuates more than above the buildings owing to their reflections in the second experiment.

3) Urban Area

Figs. 10 (a)–(e) show the photos of the third experiment, where the sensing region was the one surrounded by buildings in Osaka City University. We placed 7TRXs indoors near the exterior wall windows, which transmitted the 2.4 GHz band Wi-Fi [39] signals. The experimental site was located in an urban area, so piloting a UAV in the air was strictly prohibited, so instead of a UAV, we used a receiver (RX) attached to the top of a pole, as shown in Fig. 10 (g). Table 4 summarizes the details of the experiment.

Figs. 11 (i)–(vii) show the comparison of the full RSS map, partial RSS map, and constructed full RSS map for

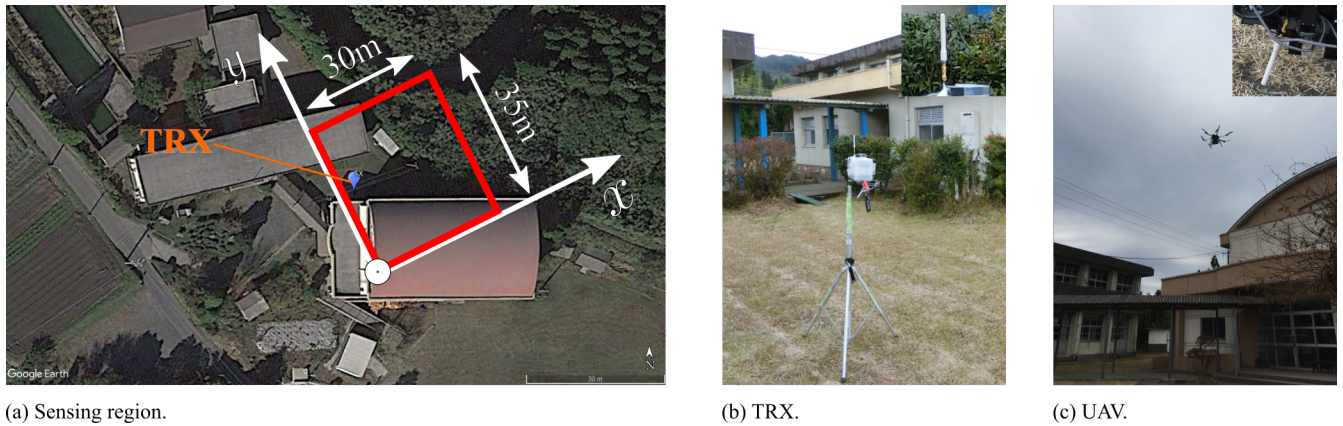


FIGURE 6. Photos of the second experiment, which was conducted in the suburban area.

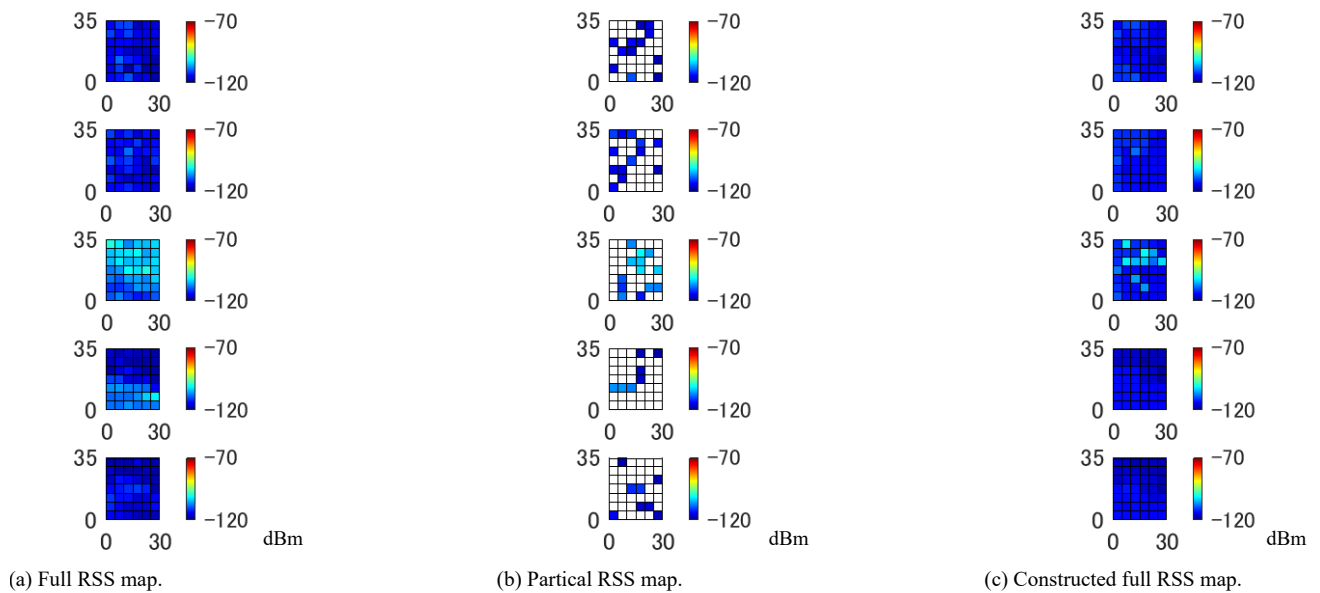


FIGURE 7. RSS maps for $E_{\text{sense}} = 0.25$ and $\lambda = 0.07$ obtained from the second experiment, which was conducted in the suburban area.

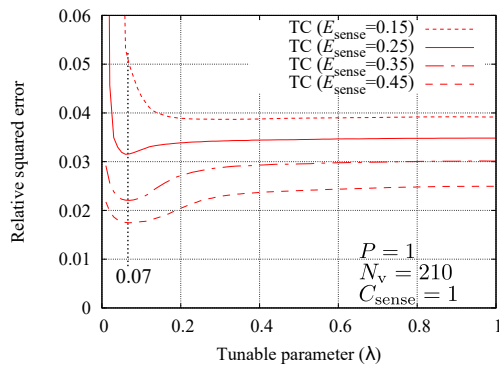


FIGURE 8. Dependency of the RSE on λ obtained from the second experiment, which was conducted in the suburban area.

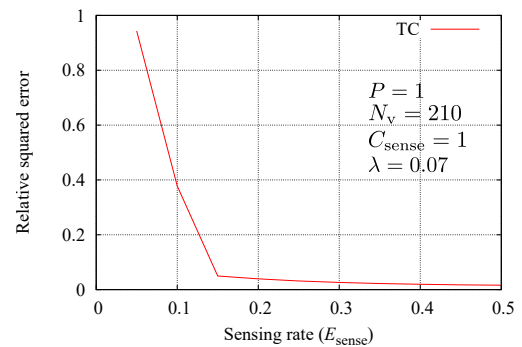


FIGURE 9. Dependency of the RSE on E_{sense} obtained from the second experiment, which was conducted in the suburban area.

the 7TRXs, where E_{sense} and λ are set to 0.25 and 0.07, respectively. Similar to the results in the first and second experiments, it seems that by sensing RSS in only 25% of

the entire region, the TC method can construct the full RSS map well.

Fig. 12 shows the dependency of the RSE on λ . No distinct

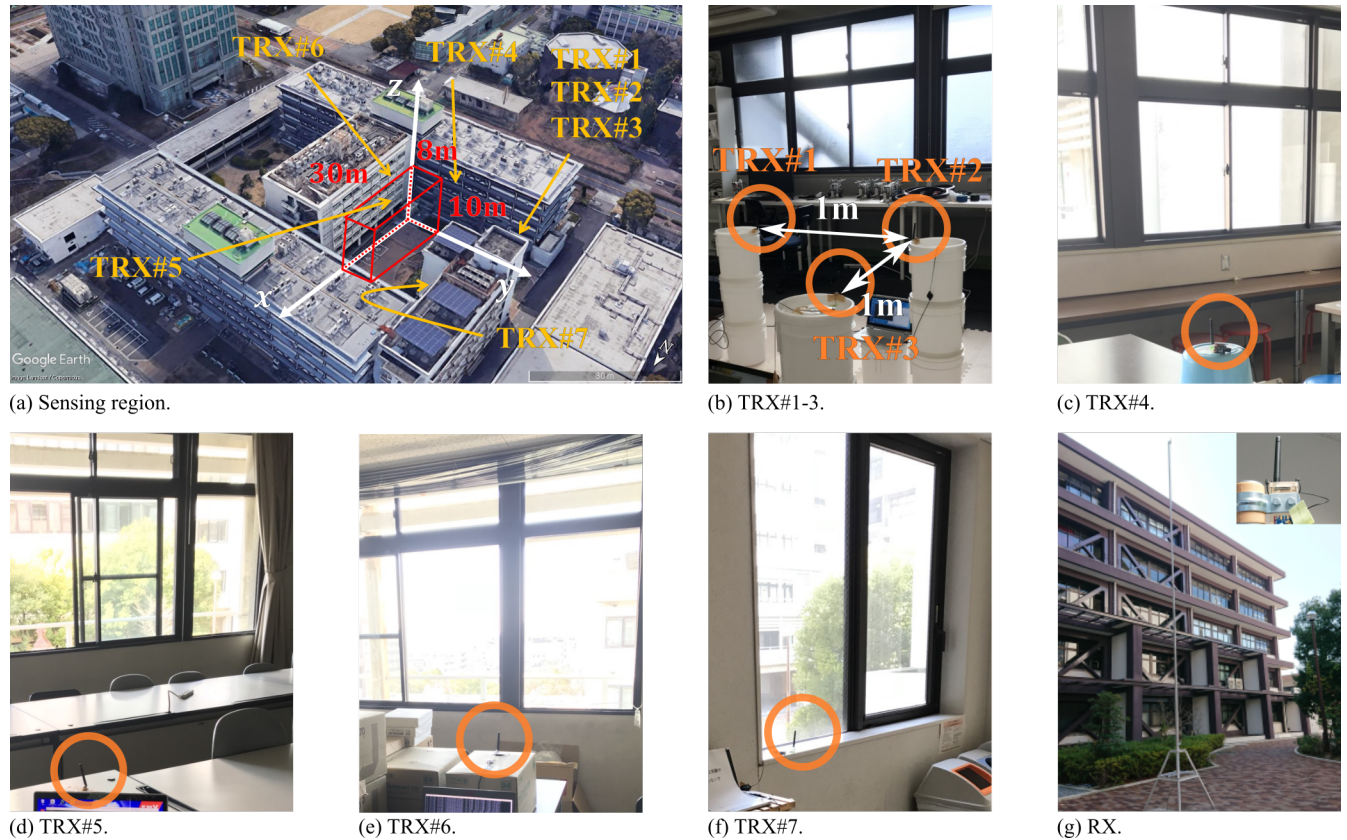


FIGURE 10. Photos of the third experiment, which was conducted in the urban area.

TABLE 4. DETAIL ON THE THIRD EXPERIMENT CONDUCTED IN THE URBAN AREA.

Location	Osaka City University
Origin of the sensing region	Latitude: $34^{\circ}35'32.98''N$ Longitude: $135^{\circ}30'14.87''E$ Altitude: 1 m
Sizes of the sensing region	$X = 30 \text{ m} \times Y = 8 \text{ m} \times Z = 10 \text{ m}$
Sensing resolution	$\Delta X = \Delta Y = \Delta Z = 2 \text{ m}$ $N_1 = 15, N_2 = 4, N_3 = 5,$ and $N_v = 300$
Number of TRXs (Q)	7
Wireless communication tool	2.4 GHz band Wi-Fi
Transmission Power	16 dBm
Antenna	Vertically polarized dipole antenna
Antenna gain	2.1 dBi

λ , which minimizes the RSE is present, but λ of around 0.1 is a proper choice for reducing the RSE. Fig. 13 shows the dependency of the RSE on E_{sense} , where E_{sense} more than 0.2 can make the RSE flat. At $E_{\text{sense}} = 0.25$ and $\lambda = 0.07$, we obtained RSE = 0.050 for the third experiment, whereas RSE = 0.017 and RSE = 0.032 for the first and second experiments, respectively.

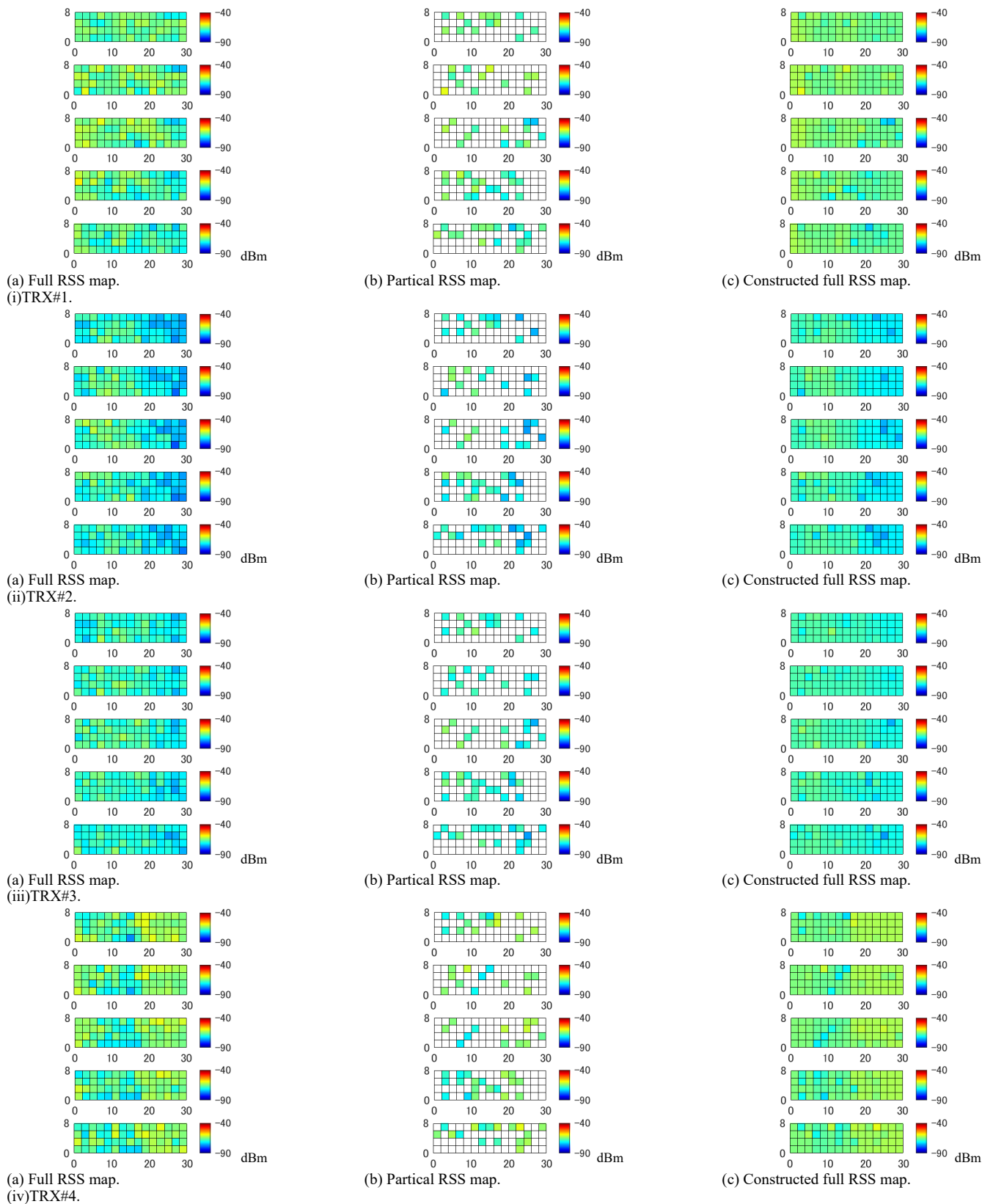
Fig. 14 shows L_{total} versus E_{sense} for the RSS sensing stage, where we solved the TSP with the genetic algorithm solver in the MATLAB global optimization toolbox [40]. It is quite natural that L_{total} increases as E_{sense} increases, and the PS method with $E_{\text{sense}} = 0.25$ can make L_{total} less than

one-third of that for the FS method. In the following, we set $E_{\text{sense}} = 0.25$ and $\lambda = 0.07$, and this is also the reason why we set so in Figs. 3, 7, and 11.

Fig. 15 shows T_{total} versus Q , where we assumed $D = 100 \text{ MB}$ and $f(R(\mathbf{w}_q, \mathbf{t}^p))$ was in Mbps for the IEEE 802.11-2016 standard (20 MHz band) as [41]:

$$f(R(\mathbf{w}_q, \mathbf{t}^p)) = \begin{cases} 6.5 & (-82 \leq R(\mathbf{w}_q, \mathbf{t}^p) < -79) \\ 13.0 & (-79 \leq R(\mathbf{w}_q, \mathbf{t}^p) < -77) \\ 19.5 & (-77 \leq R(\mathbf{w}_q, \mathbf{t}^p) < -74) \\ 26.0 & (-74 \leq R(\mathbf{w}_q, \mathbf{t}^p) < -70) \\ 39.0 & (-70 \leq R(\mathbf{w}_q, \mathbf{t}^p) < -66) \\ 52.0 & (-66 \leq R(\mathbf{w}_q, \mathbf{t}^p) < -65) \\ 58.5 & (-65 \leq R(\mathbf{w}_q, \mathbf{t}^p) < -64) \\ 65.0 & (-64 \leq R(\mathbf{w}_q, \mathbf{t}^p)) \end{cases} \quad (34)$$

We solved the GCP with the MATLAB optimization toolbox. In Fig. 15, since the FS/BS method gives the performance lower-bound, we can see that for the experimental layout, the UAV can collect and deliver all messages for the 7 TRXs almost in the shortest time at 2 or 3 points ($Q = 2$ or 3) if they are adequately selected. Comparing the performances by the FS method by setting $M = N_v$ and $C_{\text{sense}} = 1$, we found that there is no large difference in T_{total} between the FS/BS and FS/CO methods, so the CO method can find truly adequate message collection and delivery points for all TRXs while reducing computational complexity. T_{total} by the 25%-



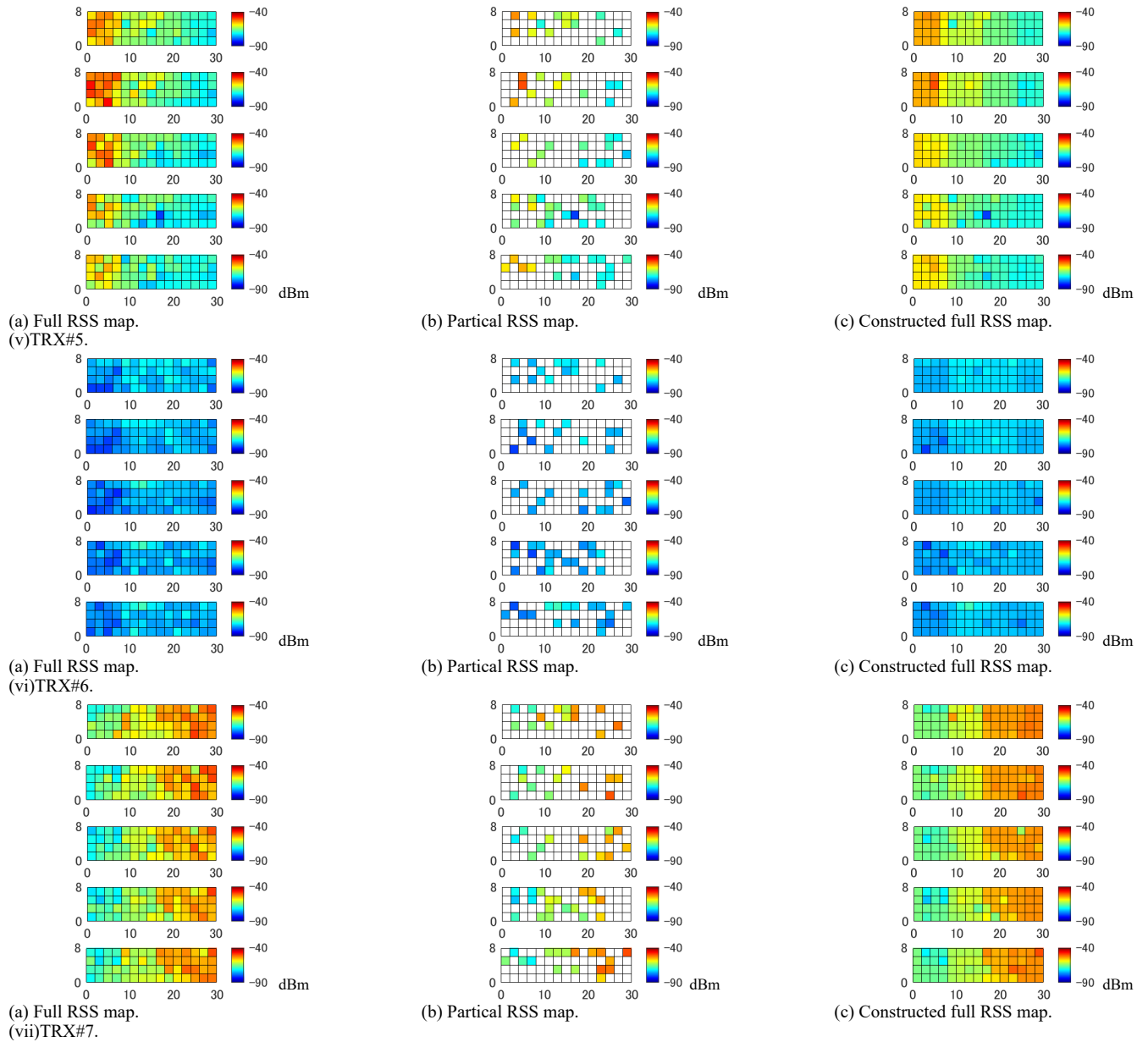


FIGURE 11. RSS maps for $E_{\text{sense}} = 0.15$ and $\lambda = 0.07$ obtained from the third experiment, which was conducted in the urban area.

PS method tends to be longer than that by the FS method, but there is no difference between them at $Q = 1$. Since T_{total} by the PS/TC/CO method is a little longer than that obtained by the PS/CO method for $Q \geq 3$, the TC method is effective when selecting the number of message collection and delivery points much smaller than that of TRXs.

Fig. 16 shows the message collection and delivery probability versus C_{sense} . As C_{sense} decreases from 1.0, since the number of points decreases where the UAV can collect messages jointly for multiple TRXs, the message collection and delivery probability decreases, especially more abruptly for smaller Q . Moreover, since the TC method constructs full RSS maps for all TRXs, it can always collect and deliver all the messages, even for lower C_{sense} .

Figs. 17 and 18 show the comparison of the dependency of T_{total} on C_{sense} between the PS/CO and PS/TC/CO methods. For the PS/CO method, as Q decreases, C_{sense} increases, and T_{total} goes to infinity. For the PS/TC/CO method, with its full RSS map constructability, it can always keep T_{total} finite. However, for lower C_{sense} , since the TC method wrongly constructs full RSS maps, T_{total} becomes longer, approaching 180 s.

Finally, Fig. 19 shows the total route length required for all message collection and delivery versus Q . We can see from this figure that the total route length when the UAV collects and delivers messages at 2 or 3 points ($Q = 2$ or 3) can be less than one-sixth or half of the one when the UAV collects and delivers messages at a different point for each TRX ($Q =$

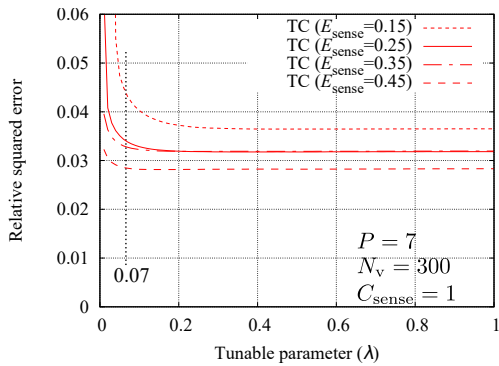


FIGURE 12. Dependency of the RSE on λ obtained from third experiment, which was conducted in the urban area.

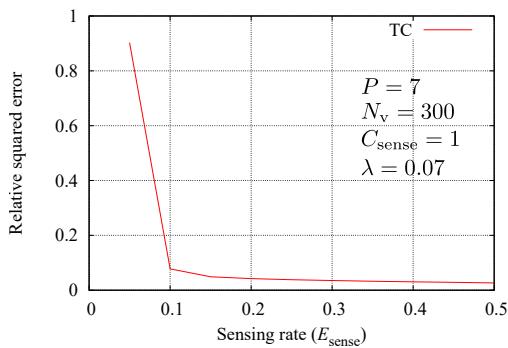


FIGURE 13. Dependency of the RSE on E_{sense} obtained from third experiment, which was conducted in the urban area.

7).

VIII. CONCLUSION

In this work, we proposed a method for the 3D determination of message collection and delivery locations for UAV-enabled disaster recovery networks. Our method is based on two functions: the 3D RSS map construction based on tensor completion and the message collection and delivery location determination based on the correlation calculation of RSS maps. The theoretical analysis of the computational complexity revealed that the proposed method can reduce the computational order in terms of the number of algorithm steps compared to the brute search-based method. Furthermore, the experimental performance evaluation conducted in the rural, suburban, and urban areas revealed that the proposed method can save time and energy while constructing 3D RSS maps and determine the message collection and delivery locations using the constructed 3D RSS maps.

We have conducted experiments in small sensing areas since it is likely that a dense TRX occurs, even in small sensing areas, if there are multiple TRXs in a shelter or a shelter is located next to another. In the future, we will conduct more experiments in a larger area in addition to experiments using a UAV in urban areas. Furthermore, we need to tackle the problem of joint determination of a cyclic route and message collection and delivery locations to minimize the total energy

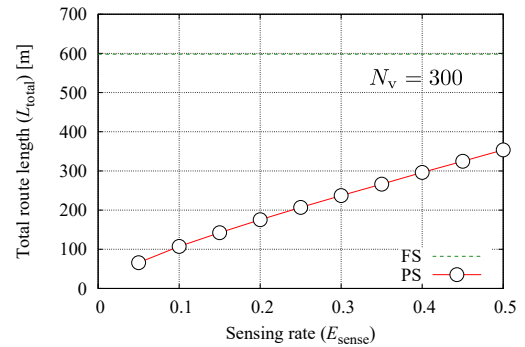


FIGURE 14. Dependency of L_{total} on E_{sense} obtained from the third experiment, which was conducted in the urban area.

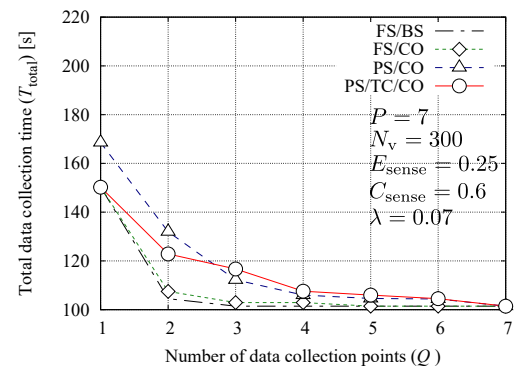


FIGURE 15. Dependency of T_{total} on Q obtained from the third experiment, which was conducted in the urban area.

consumption. In addition, data transmission technologies with multiple antennas could be used in UAV-based disaster recovery networks. For example, MIMO techniques not only increase the data transmission rate but also enable the UAV to collect and deliver messages simultaneously from/to TRXs deployed in different shelters.

APPENDIX A COMPUTATIONAL COMPLEXITY OF BS METHOD

The number of ordered arrangements of Q points selected out of M points is given by

$$N_{\mathbf{W}} = {}_M P_Q. \quad (35)$$

In addition, the number of partitioning \mathbf{S} with P elements into Q non-empty subsets is given by the Sterling number of the second kind as [42]

$$N_{\Sigma} = \frac{1}{Q!} \sum_{n=1}^Q (-1)^{Q-n} {}_Q C_n n^P. \quad (36)$$

For each combination of \mathbf{W} and Σ with the total number of $N_{\mathbf{W}} \times N_{\Sigma}$,

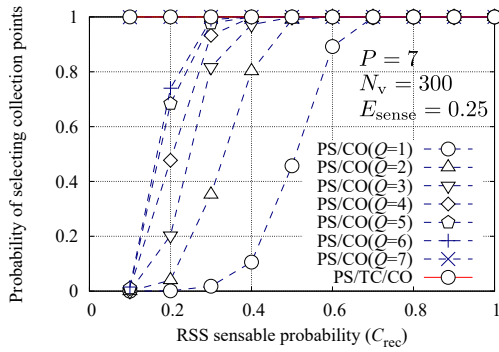


FIGURE 16. Message collection/delivery probability versus C_{sense} obtained from the third experiment, which was conducted in the urban area.

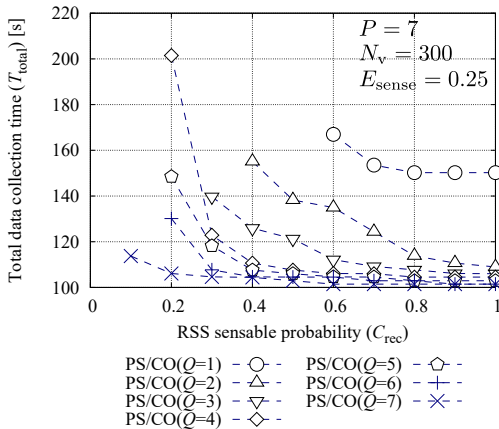


FIGURE 17. Dependency of T_{total} on C_{sense} using the PS/CO method obtained from the third experiment, which was conducted in the urban area.

- Finding a minimal RSS for the TRXs labeled with S_q requires $P_q - 1$ steps ($1 \leq q \leq Q$), so from (2), the number of steps for (20) is calculated as

$$N_{min} = \sum_{q=1}^Q (P_q - 1) = P - Q. \quad (37)$$

- The number of steps for (19) is written as

$$N_{add} = Q - 1. \quad (38)$$

Furthermore, finding the maximal R in (18) requires steps of

$$N_{max} = N_{\mathbf{W}} \times N_{\Sigma} - 1, \quad (39)$$

so from (35)–(39), the number of steps for the BS method is written as

$$N_{BF} = (N_{min} + N_{add}) \times N_{\mathbf{W}} \times N_{\Sigma} + N_{max}. \quad (40)$$

The computational order of $N_{\mathbf{W}}$ is given by

$$O_{\mathbf{W}} = O(M^Q), \quad (41)$$

and N_{Σ} is lower-bounded by

$$N_{\Sigma} \geq 1, \quad (42)$$

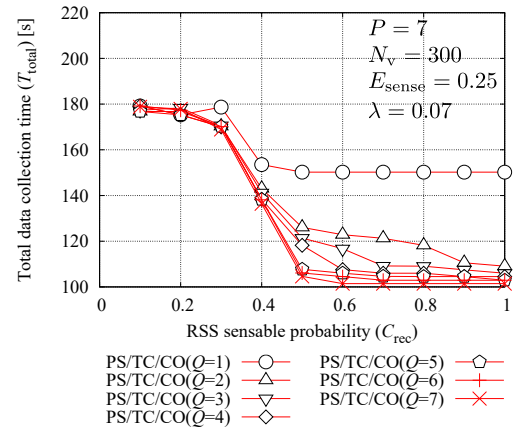


FIGURE 18. Dependency of T_{total} on C_{sense} using the PS/TC/CO method obtained from the third experiment, which was conducted in the urban area.

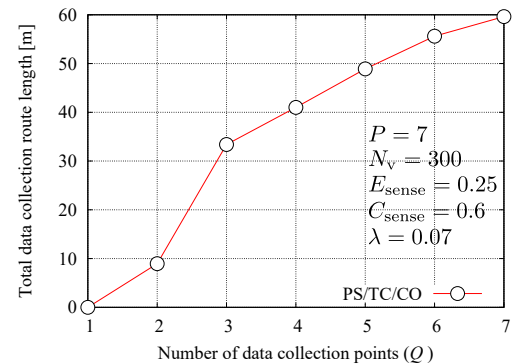


FIGURE 19. Total route length for message collection and delivery versus Q obtained from the third experiment, which was conducted in the urban area.

so substituting (37)–(39), (41), and (42) into (40), the computational order of the BS method is finally lower-bounded by

$$O_{BF} = O(P \times M^Q). \quad (43)$$

APPENDIX B FORMULATION OF CO METHOD AS A GRAPH COLORING PROBLEM (GCP)

We consider an undirected graph, where vertexes are composed of TRXs. The set of vertexes is given by

$$\mathbf{V} = \{v_p | 1 \leq p \leq P\} \quad (44)$$

and the adjacency matrix is given by

$$\mathbf{A} = \{a_{pp'} | 1 \leq p, p' \leq P\} \quad (45)$$

$$a_{pp'} = \begin{cases} 0 & (\rho(\mathbf{R}^p, \mathbf{R}^{p'}) \geq \rho_{th}) \\ 1 & (\rho(\mathbf{R}^p, \mathbf{R}^{p'}) < \rho_{th}) \end{cases}, \quad (46)$$

which means that edges connect only vertexes with lower correlations. The decomposition problem is transformed into

a GCP to partition \mathbf{V} into Q non-empty subsets whose elements are not connected with edges as

$$\text{find } \hat{\Sigma} \text{ which satisfies} \\ a_{pp'} = \begin{cases} 1 & (p \in \mathbf{S}_q, p' \in \mathbf{S}_{q'}, q \neq q') \\ 0 & (p \in \mathbf{S}_q, p' \in \mathbf{S}_{q'}, q = q') \end{cases}. \quad (47)$$

For an \mathbf{A} , which is determined by a given ρ_{th} , the GCP may give no solution, so we need to repeatedly solve it until it gives a solution by changing \mathbf{A} through $\rho_{\text{th}} \leftarrow \rho_{\text{th}} + \Delta\rho$ ($0 < |\Delta\rho| < 1$).

Now, let us consider the computational complexity when applying a BS method to the GCP. The number of partitioning P vertexes into Q subsets is given by (36), which is upper-bounded by [43]

$$N_{\Sigma} \leq \frac{1}{2} P C_Q Q^{P-Q}, \quad (48)$$

and the number of examining any pairs of vertexes whether they have an edge or not is written as

$$N_{\text{exam}} = P C_2. \quad (49)$$

In addition to these, when applying a bisection method to search a solution with a higher ρ_{th} , the maximal number of iterations is given by [44]

$$N_{\text{itl}} = \log_2(2/|\Delta\rho|) = 1 - \log_2 |\Delta\rho|. \quad (50)$$

The number of steps for solving the GCP is given by multiplication of N_{Σ} , N_{exam} , and N_{itl} , so from (48), (49), and (50), its computational order is upper-bounded by

$$O_{\text{gcp}} = P^{Q+2} \times Q^{P-Q} \times (1 - \log_2 |\Delta\rho|). \quad (51)$$

APPENDIX C COMPUTATIONAL COMPLEXITY OF CO METHOD

First of all, (24) contains additions, subtractions, multiplications, and a division, but from (25), the number of steps for the correlation evaluation is upper-bounded by

$$N_{\rho} \propto \sum_{p=1}^{P-1} \sum_{p'>p}^P |\mathbf{B}^p \cap \mathbf{B}^{p'}| \leq P C_2 M. \quad (52)$$

Secondly, the order of solving the GCP is given by (51). Thirdly, in (26) and (27), for a given $\hat{\mathbf{S}}_q$, finding a minimal RSS requires $P_q - 1$ steps at \mathbf{w}_q ($1 \leq q \leq M$), and finding a maximal RSS among them requires $M - 1$ steps, so the number of total required steps becomes

$$N_{\text{min-max}} = \sum_{q=1}^Q \{(P_q - 1)M + (M - 1)\} = PM - Q. \quad (53)$$

Consequently, from (52), (51), and (53), taking $M \gg P, Q$ and $|\log_2 |\Delta\rho||$, the computational order of the CO method is upper-bounded by

$$O_{\text{CO}} = O(P^2 \times M). \quad (54)$$

APPENDIX D DETERMINATION OF THE 3D SPATIAL SAMPLING RESOLUTIONS

For the wireless signals with carrier frequencies of more than 800 MHz, it is well-known that the auto-correlation function of shadow fading in land mobile communications has a single exponential decay with a decorrelation distance of d_{decor} . Typical values of d_{decor} are listed in [45], such as 37 m (rural macromodel), 40 m (suburban macromodel), and 37 m (urban macromodel), so (1) is satisfied when setting ΔX , ΔY , and $\Delta Z < 10$ m.

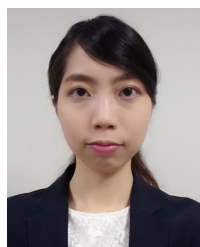
ACKNOWLEDGEMENT

We would like to acknowledge Prof. Shingo Ata of Osaka City University, Japan for his great support.

REFERENCES

- [1] J. Hansen, M. Sato, R. Ruedy, A. Lacis, and V. Oinas, "Global warming in the twenty-first century: An alternative scenario," *Proc. Natl. Acad. Sci. USA*, vol. 97, no. 18, pp. 9875–9880, Aug. 2000, doi: 10.1073/pnas.170278997.
- [2] Ministry of Internal Affairs and Communications of Japan, "Impact of the Great East Japan Earthquake on telecommunications and broadcasting services and associated response," (in Japanese), 2011. [Online]. Available: <http://www.bousai.go.jp/oukyu/higashinihon/4/pdf/soumu.pdf>
- [3] Q. Wu *et al.*, "5G-and-beyond networks with UAVs: From communications to sensing and intelligence," *IEEE J. Sel. Areas Commun. (J-SAC)*, 2021, arXiv: 2010.09317.
- [4] A. M. Hayajneh, S. A. R. Zaidi, D. C. McLernon, M. D. Renzo and M. Ghogho, "Performance analysis of UAV enabled disaster recovery networks: A stochastic geometric framework based on cluster processes," *IEEE Access*, vol. 6, pp. 26215–26230, May 2018, doi: 10.1109/ACCESS.2018.2835638.
- [5] G. B. Dantzig and J. H. Ramser, "The truck dispatching problem," *Management Sci.*, vol. 6, no. 1, pp. 80–91, 1959, doi: 10.1287/mnsc.6.1.80.
- [6] P. Toth and D. Vigo, *The Vehicle Routing Problem*. SIAM, Philadelphia, PA, USA, 2002.
- [7] DJI, <https://www.dji.com>.
- [8] M. Takai, J. Martin, S. Kaneda, and T. Maeno, "Scenargie as a network simulator and beyond," *J. Inf. Process.*, vol. 27, pp. 2–9, 2019, doi: 10.2197/ipsjjip.27.2.
- [9] A. Filippone, *Flight Performance of Fixed and Rotary Wing Aircraft*. Elsevier, Amsterdam, The Netherlands; New York, NY, USA, 2006.
- [10] M. Mozaffari, W. Saad, M. Bennis and M. Debbah, "Unmanned aerial vehicle with underlaid device-to-device communications: Performance and tradeoffs," *IEEE Trans. Wireless Commun.*, vol. 15, no. 6, pp. 3949–3963, Jun. 2016, doi: 10.1109/TWC.2016.2531652.
- [11] G. Tuna, B. Nefzi, and G. Conte, "Unmanned aerial vehicle-aided communications system for disaster recovery," *J. Netw. Comput. Appl.*, vol. 41, pp. 27–36, May 2014, doi: 10.1016/j.jnca.2013.10.002.
- [12] A. A. Hourani, S. Kandeepan, and S. Lardner, "Optimal LAP altitude for maximum coverage," *IEEE Wireless Commun. Lett.*, vol. 3, no. 6, pp. 569–572, Dec. 2014, doi: 10.1109/LWC.2014.2342736.
- [13] M. Mozaffari, W. Saad, M. Bennis, and M. Debbah, "Efficient deployment of multiple unmanned aerial vehicles for optimal wireless coverage," *IEEE Commun. Lett.*, vol. 20, no. 8, pp. 1647–1650, Aug. 2016, doi: 10.1109/LCOMM.2016.2578312.
- [14] M. Alzenad, A. E. Keyi, F. Lagou, and H. Yanikomeroglu, "3-D placement of an unmanned aerial vehicle base station (UAV-BS) for energy-efficient maximal coverage," *IEEE Wireless Commun. Lett.*, vol. 6, no. 4, pp. 434–437, Aug. 2017, doi: 10.1109/LWC.2017.2700840.
- [15] E. Kalantari, H. Yanikomeroglu, and A. Yongacoglu, "On the number and 3D placement of drone base stations in wireless cellular networks," *Proc. 2016 IEEE 84th Veh. Technol. Conf. (VTC2016-Fall)*, Montreal, QC, pp. 1–6, 2016, doi: 10.1109/VTCFall.2016.7881122.
- [16] J. Wang, C. Jiang, Z. Wei, C. Pan, H. Zhang, and Y. Ren, "Joint UAV hovering altitude and power control for space-air-ground IoT networks," *IEEE Internet Things J.*, vol. 6, no. 2, pp. 1741–1753, April 2019, doi: 10.1109/IIOT.2018.2875493.

- [17] J. Wang, C. Jiang, Z. Han, Y. Ren, R. G. Maunder, and L. Hanzo, "Taking drones to the next level: Cooperative distributed unmanned-aerial-vehicular networks for small and mini drones," *IEEE Veh. Technol. Mag.*, vol. 12, no. 3, pp. 73–82, Sep. 2017, doi: 10.1109/MVT.2016.2645481.
- [18] J. Zhang, E. Björnson, M. Matthaiou, D. W. K. Ng, H. Yang, and D. J. Love, "Prospective multiple antenna technologies for beyond 5G," *IEEE J. Sel. Areas Commun.*, vol. 38, no. 8, pp. 1637–1660, Aug. 2020, doi: 10.1109/JSAC.2020.3000826.
- [19] A. Otto, N. Agatz, J. Campbell, B. Golden, and E. Pesch, "Optimization approaches for civil applications of unmanned aerial vehicles (UAVs) or aerial drones: A survey," *Networks*, vol. 72, no. 4, pp. 411–458, Mar. 2018, doi: 10.1002/net.21818.
- [20] A. Thibbotuwawa, G. Bocewicz, P. Nielsen, and Z. Banaszak, "Unmanned aerial vehicle routing problems: A literature review," *Appl. Sci.*, vol. 10, no. 13, Art. no. 4504, Jun. 2020, doi: 10.3390/app10134504.
- [21] T. S. Alemayehu and J. H. Kim, "Efficient nearest neighbor heuristic TSP algorithms for reducing data acquisition latency of UAV relay WSN," *Wireless Pers. Commun.*, vol. 95, no. 3, pp. 3271–3285, Aug. 2017, doi: 10.1007/s11277-017-3994-9.
- [22] C. Zhan, Y. Zeng, and R. Zhang, "Energy-efficient data collection in UAV enabled wireless sensor network," *IEEE Wireless Commun. Lett.*, vol. 7, no. 3, pp. 328–331, Jun. 2018, doi: 10.1109/LWC.2017.2776922.
- [23] D. T. Ho, E. I. Grøtli, P. B. Sujit, T. A. Johansen, and J. B. Sousa, "Optimization of wireless sensor network and UAV data acquisition," *J. Intell. Robot. Syst.*, vol. 78, no. 1, pp. 159–179, Apr. 2015, doi: 10.1007/s10846-015-0175-5.
- [24] D. L. Applegate, R. E. Bixby, V. Chvátal, and W. J. Cook, *The traveling salesman problem: A computational study*. Princeton Univ. Press, Princeton, NJ, USA, 2006.
- [25] K. Dorling, J. Heinrichs, G. G. Messier, and S. Magierowski, "Vehicle routing problems for drone delivery," *IEEE Trans. Syst., Man, Cybern., Syst.*, vol. 47, no. 1, pp. 70–85, Jan. 2017, doi: 10.1109/TSMC.2016.2582745.
- [26] B. N. Coelho, V. N. Coelho, I. M. Coelho, L. S. Ochi, R. Haghazari, D. Zuidema, M. S. F. Lima, and A. R. da Costa, "A multi-objective green UAV routing problem," *Comput. Oper. Res.*, vol. 88, pp. 306–315, Dec. 2017, doi: 10.1016/j.cor.2017.04.011.
- [27] A. Danjo, A. Murata, S. Hara, T. Matsuda, and F. Ono, "Construction of a temporary message collection system using a drone for refugees in a large-scale disaster," in *Proc. 2020 IEEE 91st Veh. Technol. Conf. (VTC2020-Spring)*, May 2020, pp. 1–5, doi: 10.1109/VTC2020-Spring48590.2020.9128632.
- [28] A. Perez, A. Fouda, and A. S. Ibrahim, "Ray Tracing analysis for UAV-assisted integrated access and backhaul Millimeter Wave Networks," in *Proc. 2019 IEEE 20th Int. Symp. A World of Wireless, Mobile and Multimedia Networks (WoWMoM)*, Washington, DC, USA, 2019, pp. 1–5, doi: 10.1109/WoWMoM.2019.8792969.
- [29] J. Chen, U. Yatnalli, and D. Gesbert, "Learning radio maps for UAV aided wireless networks: A segmented regression approach," in *Proc. 2017 IEEE Int. Conf. Commun. (ICC)*, Paris, France, May 2017, pp. 1–6, doi: 10.1109/ICC.2017.7997333.
- [30] H. Nishioka, A. Danjo, S. Hara, T. Matsuda, F. Ono, R. Miura, and F. Kojima, "A compressed sensing-based 3D-RSS MAP completion for UAV routes planning," *Proc. 2018 12th Int. Conf. Sens. Technol. (ICST)*, Limerick, Ireland, Dec. 2018, pp. 273–277, doi: 10.1109/IC-SensT.2018.8603618.
- [31] T. Y. Ji, T. Z. Huang, X. L. Zhao, T. H. Ma, and G. Liu, "Tensor completion using total variation and low-rank matrix factorization," *Inf. Sci.*, vol. 326, pp. 243–257, Jan. 2016, doi: 10.1016/j.ins.2015.07.049.
- [32] A. Danjo, S. Hara, T. Matsuda, and F. Ono, "A tensor completion-based selection method of a single data collection point for multiple shelters in a UAV enabled disaster recovery network," *Proc. 12th Int. Conf. Adv. Satell. Space Commun. (SPACOMM 2020)*, Lisbon, Portugal, Feb. 2020, pp. 7–12.
- [33] M. Gudmundson, "Correlation model for shadow fading in mobile radio systems," *Electron. Lett.*, vol. 27, no. 23, pp. 2145–2146, Nov. 1991, doi: 10.1049/el:19911328.
- [34] J. Y. Potvin, "Genetic algorithms for the traveling salesman problem," *Ann. Oper. Res.*, vol. 63, no. 3, pp. 337–370, Jun. 1996, doi: 10.1007/BF02125403.
- [35] M. Dorigo and L. M. Gambardella, "Ant colony system: A cooperative learning approach to the traveling salesman problem," *IEEE Trans. Evol. Comput.*, vol. 1, no. 1, pp. 53–66, Apr. 1997, doi: 10.1109/4235.585892.
- [36] D. Kressner, M. Steinlechner, B. Vandereycken, "Low-rank tensor completion by Riemannian optimization," *Bit Numer. Math.*, vol. 54, pp. 447–468, Jun. 2014, doi: 10.1007/s10543-013-0455-z.
- [37] J. A. Bengua, H. N. Phien, H. D. Tuan, M. N. Do, "Efficient tensor completion for color image and video recovery: Low-rank tensor train," *IEEE Trans. Image Process.*, vol. 26, no. 5, pp. 2466–2479, May 2017, doi: 10.1109/TIP.2017.2672439.
- [38] E. Malaguti and P. Toth, "A survey on vertex coloring problems," *Int. Trans. in Oper. Res.*, vol. 17, no. 1, pp. 1–34, 2010, doi: 10.1111/j.1475-3995.2009.00696.x.
- [39] Wi-Fi Alliance, <https://www.wi-fi.org/>
- [40] MATLAB, The MathWorks, Inc. <https://www.mathworks.com/>
- [41] *IEEE Standard for Information technology – Telecommunications and information exchange between systems Local and metropolitan area networks – Specific requirements - Part 11: Wireless LAN Medium Access Control (MAC) and Physical Layer (PHY) specifications*, IEEE Std 802.11-2016 (Revision of IEEE Std 802.11-2012), Dec. 2016, doi: 10.1109/IEEESTD.2016.7786995.
- [42] D. E. Knuth, *The Art of Computer Programming, Vol.4, Fascicle 3: Generating All Combinations and Partitions*. Addison-Wesley, Reading, MA, USA, 2005.
- [43] N. M. Temme, "Asymptotic estimates of Stirling numbers," *Stud. Appl. Math.*, vol. 89, no. 3, pp. 233–243, Aug. 1993, doi: 10.1002/sapm1993893233.
- [44] M. Patel, *Data Structure and Algorithm With C*. Education Publishing, 2018.
- [45] M Series, ITU 2135-1 "Guidelines for evaluation of radio interface technologies for IMT-advanced," 2009.



AZUSA DANJO received her B.Eng. and M.Eng. degrees in information engineering from Osaka City University, Osaka, Japan, in 2014 and 2016, respectively. Since 2016, she has been with Daihen Corporation, Osaka, Japan. She is also currently pursuing a Ph.D. degree at Osaka City University. Her research interests include wireless communications and localization systems.



RYU MIURA received his B.E., M.E., and Ph.D. degrees in electrical engineering from Yokohama National University, Yokohama, Japan, in 1982, 1984, and 2000, respectively. He joined the Radio Research Laboratory, Tokyo, Japan, in 1984, which was reorganized by the National Institute of Information and Communications Technology (NICT) in 2004. He is currently the principal investigator of the Wireless Networks Research Center, NICT, Yokosuka, Japan, where he currently works on disaster-resilient wireless networks and the applications of unmanned aircraft wireless relay networks.

...



SHINSUKE HARA received his B.Eng., M.Eng. and Ph.D. degrees in communications engineering from Osaka University, Osaka, Japan, in 1985, 1987, and 1990, respectively. He was an assistant professor from April 1990 to September 1997 and an Associate Professor from October 1997 to September 2005 at Osaka University. Since October 2005, he is a professor in with the Graduate School of Engineering, Osaka City University. From April 1995 to March 1996, he was also a visiting scientist in the Telecommunications and Traffic Control Systems Group, Delft University of Technology, Delft, The Netherlands. His research interests include mobile and indoor wireless communications and digital signal processing.



TAKAHIRO MATSUDA received his B.E. (with honors), M.E., and Ph.D. degrees in communications engineering from Osaka University in 1996, 1997, 1999, respectively. He joined the Department of Communications Engineering at the Graduate School of Engineering, Osaka University in 1999. In the same department, he was an assistant professor from 1999 to 2005, lecturer from 2005 to 2009, and an associate professor from 2009 to 2018. He is currently a professor in the Department of Computer Science, Graduate School of Systems Design, Tokyo Metropolitan University. His research interests include performance analysis and the design of communication networks and wireless communications. He received the Best Tutorial Paper Award and the Best Magazine Paper Award from IEICE ComSoc in 2012, and the Best Paper Award from IEICE in 2014. He is a member of IPSJ and IEEE and a senior member of IEICE.



FUMIE ONO received her B.E., M.E., and Ph.D. degrees in electrical engineering from Ibaraki University, Japan, in 1999, 2001, and 2004, respectively. From 2004 to 2006, she was a research associate in the Faculty of Engineering, Tokyo University of Science. From 2006 to 2011, she was an assistant professor in the Division of Electrical and Computer Engineering, Yokohama National University. From April 2012 to July 2020, she was a senior researcher in the Wireless Network Research Center, National Institute of Information and Communications Technology (NICT), Japan. She received the Young Engineer Award from the IEICE in 2006 and the YRP Award from the YRP Award Committee in 2007.